Journal of Materials Chemistry A

Accepted Manuscript

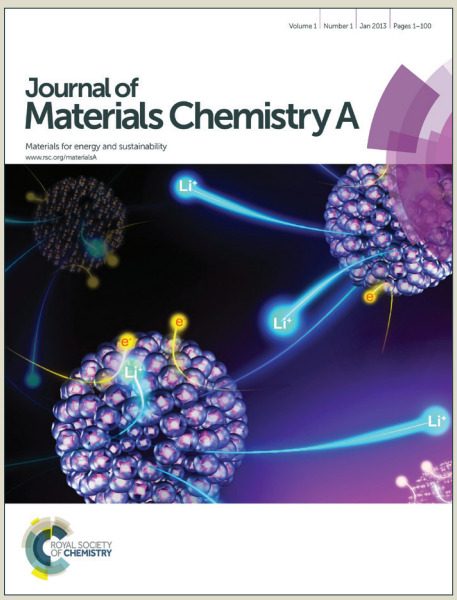

ROYAL SOCIETY OF CHEMISTRY

www.rsc.org/materialsA

H_xMoO_{3-y} nanobelts for high-performance pseudocapacitors with sea water as electrolyte and desalination device

Liang Huang ‡[a], Xiang Gao ‡ [a], Qiang Dong ‡[b], Zhimi Hu [a], Xu Xiao [a], Tianqi Li [a], Yongliang Cheng [a], Bin Yao [a], Jun Wan [a], Dong Ding [c], Zheng Ling [b], Jieshan Qiu [b] and Jun Zhou [a]*

[a] Dr. L. Huang, X. Gao, Z. M. Hu, X. Xiao, T. Q. Li, Dr. Y. L. Cheng, B. Yao, J. Wan and Prof. J. Zhou

Wuhan National Laboratory for Optoelectronics, and School of Optical and Electronic Information, Huazhong University of Science and Technology, Wuhan, 430074, China

[b] Q. Dong, Z. Ling and Prof. J. S. Qiu,

Carbon Research Laboratory, Liaoning Key Lab for Energy and Chemical Engineering, State Key Lab of Fine Chemicals, School of Chemical Engineering, Dalian University of Technology, Dalian 116024, China.

[c] Dr. D. Ding, Redox Power Systems, 387 Technology Drive, Suite 2107, College Park, Maryland 20742 USA.

*Correspending author

E-mail: jun.zhou@mail.hust.edu.cn

‡ Authors with equal contribution

Abstract Pseudocapacitors, which store charge through fast reversible redox reations occuring at the surface of electrode, could offer higher specific capacitance than electrochemical double-layer capacitors (EDLCs). However, the prime pseudocapacitive phase, transition metal oxides usually have poor electronic conductivity, limiting their practical application. Here, we fabricated highly conductive H_xMoO_{3-x} nanobelts as electrode materials for pseudocapactors. This electrode has been demonstrated great electrochemical activity in various cations aqueous solution with highest volumetric capacitance over 350 F/cm^3. Significantly, this electrode has high specific capacitance as well as excellent cycling stability in the

sea water. Moreover, this hybrid composite also exhibits remarkable ions electrosorptive capacity (4 mg/g) as desalination electrode.

Keywords: H_xMoO_{3-y} nanobelts, sea water, supercapacitors, capacitive desalination.

Introduction

Electrochemical capacitors (ECs, also denoted as "ultracapacitors" or "supercapacitors") which may deliver a burst of energy on the timescale from 10^{-1} to 10^{2} seconds have been widely used for powering now-ubiquitous portable electronics.[1] The few seconds for energy released from ECs and the magnitude of the energy release during the desired pulse of power are the two main criterias to assess the performance of an EC system.[2] Followed by the highly developed technologies, numerous applications require more energy to be delivered from ECs in seconds than that can be obtained from electrochemical double-layer capacitors (EDLCs) which store charge electrostatically from the reversible adsorption of ions onto high-surface-area active carbonaceous materials.[3] To improve the specific energy densities released by ECs, researchers have been concentrated on exploring electrode materials base on invention of novel charge-storage mechanisms globally.[4] Pseudocapacitance, which occurs reversible redox reactions at or near the surface of the electrode leads to much greater charge storage. Transition metal oxides are primary candidates as the pseudocapacitive phase, especially for the layered metal oxides which offer facile accommodation for cations (such as Li^+, Na^+, Mg^{2+} and K^+) have been drawing considerable attention. Typically, MoO_3 is a very attractive material with two dimensional layered structures of linked MoO_6 octahedra, allowing the intercalation of protons and cations to occupy spaces in the van der Waals (vdW) gaps between double layers of MoO_6 octahedra as well as intralayer sites on zigzag chains along the channels.[5] Moreover, multiple oxidation states of Mo enable sufficient redox reactions for enhancing pseudocapacitance generation. Nevertheless, the poor electronic conduction of MoO_3 restrains power delivery on the few-seconds

timescale.[6] A few recent works demonstrated two efficient ways to improve the conductivity of transition metal oxide, chemical reduction and conductive materials coating.[7] Through reduction in the acid solution, the hydrogen is capable of intercalating into the layered MoO_3 producing the hydrogen molybdenum bronze (H_xMoO_{3-y}, $0 < x < 2$) phase which has been demonstrated the metal-semiconductor transition occur at a critical temperature and possesses much higher conductivity than the pure MoO_3.[8] Similar to two dimensional layered structures of MoO_3, H_xMoO_{3-y} offers interlayer gaps for cations intercalation and promising accessible channel for electron transfer, thus holding great potential to act as highly active pseudocapactive material (Fig. 1a).

In advancement of exploring renewable green energy storage, environmental protection is an essential issue in the whole designation electronic device process.[9] The use of conventional H_2SO_4 or KOH as electrolyte presents many drawbacks limits their further application, mainly due to its environment pollution and corrosive characteristics towards the different metallic components in a ECs system. To address this issue, neutral electrolyte such as Na_2SO_4, LiCl and KCl should be more suitable for practical application, but all the chemicals may raise concerns about extra cost.[10] Sea water, a huge reward from nature mother, contains abundance of cations such as Na^+ (1.05%), Mg^{2+} (0.135%) and K^+ (0.038%) may serve as an ideal electrolyte for the ECs, especially for intercalation capacitors by perfectly combining economic benefit and environmental conservation consideration.[11] Moreover, the performance of electrode in the sea water may give a signal of electrosorptive capability for ions as desalination application.[12]

In this work, we successfully demonstrated the application of SnO_2 coated H_xMoO_{3-y} (S-H_xMoO_{3-y}) hybrid composite as highly active intercalation capacitive material in various cations aqueous solution including Li^+, K^+, Mg^{2+} and Na^+. Most importantly, this electrode exhibited great electrochemical performance in the seawater electrolyte. Also, the composite presented very rapid ion adsorption in the application of capacitive deionization.

Experimental Section

Synthesis of MoO_3 nanobelts: Molybdenum powder (99.5%), H_2O_2, HCl (38%), and tin (II) chloride (99%) were purchased from Aladdin and used as received without further purification. The Pristine MoO_3 nanobelts were synthesized via a hydrothermal process based on the previous report.[5b] 0.8 g molybdenum powder was added into 5 mL H_2O_2 solution and stirred for 10 min to achieve a transparent yellow solution. 75 ml DI water was then diluted the above solution under stirring another 10 min. The resultant solution was transferred to a Teflon-lined stainless steel autoclave and heated at 180 ℃ for 12 h. The product precipitate was filtered and rinsed with deionized water, followed by drying at 80 ℃ for 8 h. The obtained powder was further treated at 450℃ for 1h in the air.

Synthesis of S-H_xMoO_{3-y}: 0.5 g MoO_3 was ultrasonically dispersed into 50 ml distilled water for 30 minutes. 0.45 ml HCl (38%) and 0.75 g $SnCl_2 \cdot 2H_2O$ were added into the above solution. After ultrasonically treatment for 10 min and vigorously stirring for 0-3 h, the resulting precipitates were collected and washed with ethanol and distilled water. Then, the dark blue products were dried at 80 ℃ for 12 h.

Preparation of freestanding S-H_xMoO_{3-y}/CNT films: 0.4 g sodium dodecyl benzene sulfonate (SDBS) surfactant was added into 50 ml CNTs (0.021 g, Blue Nano, China) and S-H_xMoO_{3-y} (0.039 g) suspension and sonicated for 20 min. The as-obtained solution was filtered through a membrane with the 220 nm pore size and washed with DI water several times to clean up the surfactant. The obtained filter cake was dried at 70 ℃ for 4 min and then peeled off to get a freestanding film, then punched into circular electrodes. Each electrode is ~ 0.5 mg in mass, 20 μm in thickness and 5 mm in diameter with a density around 0.9 g/cm^3 (2.5 mg/cm^2)

Characterization: The morphology of S-H_xMoO_{3-y} nanobelts were analyzed by using field emission scanning electron microscope (FESEM, FEI Nova 450 Nano) and transmission electron microscope (TEM, Tecnai G20). The measurements of CV and galvanostatic charge/discharge were carried out by using CHI 660. For the typical three electrode measurement, a piece of S-H_xMoO_{3-y}/CNT films was used as work

electrode, Ag/AgCl (CHI, USA), YP-50 (Kuraray Chemical, USA) and Celgard (Celgard, USA) was used as reference electrode, counter electrode and the separator, respectively. Two-electrode symmetric device was constructed based on two pieces of S-H_xMoO_{3-y}/CNT films with same area and mass as electrode. All the electrochemical tests were conducted in Swagelok cells (Swagelok, USA). Electrochemical impedance was performed by using Autolab PGSTAT302N measured from 10 mHz to 1 MHz with a potential amplitude of 10 mV. All the capacitance calculation just base on the mass loading of metal oxide.

Capacitive deionization test: The electrosorption capacity of the CDI system with the MoO_3/CNT hybrid film electrode was conducted in a continuously recycling system including a self-made CDI unit, a electrochemical working station (CHI760E, Shanghai Chenhua, China), a conductivity meter (ET915, eDAQ TECH, Australia), a pump (BT100-2J, Baoding LanGe constant Flow Pump Co., LTD, China) and two water tanks. In each experiment, the NaCl solution was continuously pumped from the pump into the cell and the effluent was collected into another the tank. The electrical conductivity variation of the outlet stream is monitored in real time by using the ion conductivity meter. In detail, the experiment was performed at the volume flow rate of 4 mL /min, the distance between the electrodes was 1 mm, the adsorption and desorption time is 20 min, and a direct voltage of 0.4-1.6 V with an interval of 0.4 V was applied. In the present work, the electrosorption capacity (Q, mg g^{-1}) was calculated by the equation shown below:

$$Q = \frac{(C_0 - C_e) \cdot V}{m}$$

where C_0 and C_e are the initial and equilibrium concentration (mg/L), respectively, V is the volume of the solution (L), and m is the total mass of the electrodes (g).

Results and Discussion

The S-H_xMoO_{3-y} nanobelts were obtained through one simple step by using $SnCl_2$ to reduce the MoO_3 nanobelts in the acid solution under room temperature. The as-synthesized product is firstly characterized by X-ray diffraction (XRD) to identify

its crystalline structure. As can be seen from Fig. 1b-c, all of the diffraction peaks can be assigned to orthorhombic MoO_3 (JCPDS card no. 05–0508) before reduction reaction. After treated with $SnCl_2$, the 2θ values of the diffraction peaks corresponding to (020), (040) and (060) decrease gradually following the continuous reaction time. After 1 h reaction, the 2θ value was almost consistent, suggesting complete reduction. The smaller 2θ value means larger interplane distance (d value), according to Bragg Formula $2d \sin\theta = \lambda$. It should be noted that there is no obvious peak corresponding to the SnO_2 because several characteristic peaks of SnO_2 are very close to the peaks of orthorhombic MoO_3. The detailed morphology and structural features of S-H_xMoO_{3-y} were further characterized by scanning electron microscope (SEM) and Transmission electron microscope (TEM). The typical SEM image of S-H_xMoO_{3-y} is shown in the Fig. 1d, suggesting its belt structure with length of 3-6 μm and thickness of ~40 nm. Element mapping from the scanning TEM (STEM) is carried out to identify the element distribution. As shown in the Fig. 1e, elements of oxygen, molybdenum and tin are clearly detected in the single S-H_xMoO_{3-y} nanobelt. The X-ray photoelectron spectra (XPS) analysis also confirms these three elements consist of the composite of S-H_xMoO_{3-y} (Fig. S1‡). Besides, the doublets of 231.6 and 234.7 eV are attributed, respectively, to the binding energies of the $3d^{5/2}$ and $3d^{3/2}$ electrons of Mo^{4+}, which are present in S-H_xMoO_{3-y} nanobelts. The ratio of Mo^{4+}/Mo^{6+} on surface reach as high as 72.2%, indicating a strong reduction occurs. The HRTEM image shows the crystalline phase of the S-H_xMoO_{3-y} nanobelt, also giving a vision of the small SnO_2 crystal coating on the H_xMoO_{3-y} surface. An interplaner spacing of 0.4 nm was obtained from the HRTEM resolved lattice fringes and corresponded to the (001) interplanar of H_xMoO_{3-y} (Fig. 1f), the interplanar spacing of 0.31 nm is in agreement with the SnO_2 crystal.[13] As was expected, this small SnO_2 crystal may help create accessible sites for charge transfer on the surface of H_xMoO_{3-y} nanobelt.

To evaluate the electrochemical performances of S-H_xMoO_{3-y} hybrid composite under different reaction time, cyclic voltammetry (CV) and galvanostatic charge-discharge (GCD) were conducted in a three-electrode configuration with 5 M

LiCl as electrolyte. The different reduction time of 0.5 h, 1 h and 2 h was described as the sample of 0.5S-H_xMoO_{3-y}, 1S-H_xMoO_{3-y} and 2S-H_xMoO_{3-y}, respectively. All electrodes were fabricated by mixing the S-H_xMoO_{3-y} nanobelts and carbon nanotubes (CNTs) to prepare free standing film through the method which was described in our previous work (Fig.S2 ‡).[7d] The 1S-H_xMoO_{3-y} exhibits the highest specific capacitance over 320 F/g at the current density of 1 A/g among various samples based on the mass loading of metal oxide (Fig. S3‡). Even more impressive, the volumetric capacitance value recorded for 1S-H_xMoO_{3-y} is about308 F/cm^3 at 1 A/g. It also shows very high rate capability, the specific capacitance decreased less than 45% as the current density increased from 1 to 50 A/g (Fig. 2a). This high capacitance and remarkable rate capability are responsible for 1S-H_xMoO_{3-y} as active material for the entire following testing.

The CV area of 1S-H_xMoO_{3-y} has a dramatic increase compare to the pristine MoO_3 under the sweep rate of 5 mV/s, suggesting the enhancement of capacitance (Fig. 2b). Two pair of redox peaks exist in the CV curve of 1S-H_xMoO_{3-y} correspond to Li^+ intercalation-redox reaction process. According to previous report[6], these charge-insertion sites can be described as intralayer (b*/b) and interlayer (a*/a) Li^+ insertion/extraction, respectively. The specific capacitance of 1S-H_xMoO_{3-y} at current density of 10 A/g is 220 F/g, about 4 times the capacitance of pristine MoO_3 (Fig.S6 ‡).

Compared to the pristine MoO_3, 1S-H_xMoO_{3-y} was demonstrated much greater capacitive activation. To identify the factor required for the energy storage performance enhancement of 1S-H_xMoO_{3-y}, focused ion beam (FIB) lithography was employed to fabricate single-nanobelt device to characterize the change of conductivity between 1S-H_xMoO_{3-y} and pristine MoO_3. Fig. 2c depicts the *I-V* curves of these two samples at room temperature. The *I-V* linearity shows the two samples follow the ohmic behavior, by which the calculated electronic conductivity of pristine MoO_3 and1S-H_xMoO_{3-y} are about 14 S/m and 1350 S/m, respectively. It is obvious that highly reduction and protons insertion lead a huge promotion conductance of 1S-H_xMoO_{3-y}. Accordingly, the high performance of the 1S-H_xMoO_{3-y} is attributed to

the following unique features of the electrode. First, the high conductivity of 1S-H_xMoO_{3-y} nanobelt allows rapid access for electron transfer from the active material surface. Second, the increase of the distance between crystalline planes of (0k0) could supply more accessible channels for rich cation intercalation, leading to faster kinetics and higher utilization of active material. To understand other cations intercalation behavior for 1S-H_xMoO_{3-y}, CVs of this hybrid composite electrode in various cations aqueous solutions (K^+, Na^+ and Mg^{2+}) were also investigated in the three electrodes cell. As described in the Fig. 2d, two pair redox peaks in the CV curves of 1S-H_xMoO_{3-y} in the NaCl and KCl correspond to Na^+ or K^+ insertion/extraction the intralayer (II*/II or IV*/IV) and interlayer (I*/I or III*/III) of the matrix. In the MgSO4, one pair redox peak can be described as interlayer (V*/V) Mg^{2+} insertion/extraction because of the large cation radius of Mg^{2+}. The cathodic peak at -0.2~-0.4 V in the different electrolyte can be attributed to an irreversible phase transition,which has been shown to cause a pronounced expansion of the interlayer spacing. The different peak positions and intensities in the Fig 2d indicate different cation-intercalation processes because of their different cation radius with different diffusion kinetics.

Owing to the abundance of cations such as Na^+, Mg^{2+} and K^+ exist in the sea water. It is imaginable that the hybrid composite of the 1S-H_XMoO_{3-y} may own promising electrochemical performance in this electrolyte. The electrochemical behavior of the 1S-H_xMoO_{3-y} and pristine MoO_3 was also evaluated in the three electrodes cell system with sea water as electrolyte. Electrochemical impedance spectroscopy (EIS) was first employed to reveal conductivity difference between the 1S-H_xMoO_{3-y} and pristine MoO_3 (Fig. 3a). The diameter of the semicircle at the high frequency region of samples decreased from 14.5 Ω (MoO_3) to 4.5 Ω (1S-H_xMoO_{3-y}), directly demonstrating lower charge-transfer resistance of 1S-H_xMoO_3 which also match with *I-V* testing of the single-nanobelt devices. The volumetric capacitance of 1S-H_xMoO_{3-y} at 1 A/g achieves 210 F/cm^3 (specific capacitance base on the mass is about 250 F/g) is around 8 times of the capacitance of pristine MoO_3 (Fig. 3b-c). This value is comparable to those found for activated graphene (60 to 270 F/cm^3) or

micrometer-thin carbide-derived carbon electrodes (180 F/cm^3).[3a,14] Moreover, this hybrid composite also holds good rate capability of 48.7% when the current density increases from 1 A/g to 20 A/g. The cycling stability of 1S-H_xMoO_{3-y} was evaluated at a current density of 1 A/g in the potential range of -0.9 to -0.1 V. As shown in Fig.3d, the capacitance retention of 93.3% after 4000 cycles demonstrates the high stability of this hybrid composite. In addition, two electrodes symmetric device with sea water as electrolyte was carried out to study the potential for practical application. The Ragone plot calculated from the CDG curves displays this device gains the highest energy density of 1.1 mWh/cm^3 with a power density of 6.8 W/cm^3, which is higher than those liquid symmetric device listed in the Fig. S7.

Capacitive deionization (CDI), operating with low external power supply and energy consumption have been triggered a significant interest as an alternative method to a reverse osmosis for both static and mobile water desalination and purification applications.[16] In most case, CDI was based on the principle of EDLC to electro-absorb salt ions from the aqueous and store them on the electrical double-layer region by using high surface area carbonaceous electrode.[17] Despite these recent advances, develop new CDI mechanism to reduce the cost of CDI technology is still needed. It is believable that H_xMoO_{3-y} with ion intercalation capacitive behavior may be well-suited for CDI technology. The typical CDI experiment was conducted in the 0.5 M NaCl with a flow rate of 4 ml/min by using the 1S-H_xMoO_{3-y}/CNT film as electrode (Fig. 4 a-b). Fig. 4c shows the electrosorption-desorption cycles and the corresponding current response for this hybrid electrode on applying a cell voltage ranging from 0.4 to 1.6 V. In all cases, the conductivity of salty solution decreased quickly at the beginning of CDI processes, demonstrating a fast electrosorption of salty ions on electrode. With continuous time, the conductivity of solution decreases slowly, and reached to a stable value, suggesting an electrosorption equilibrium at the electrode. The electrosorptive capacity of 1S-H_xMoO_{3-y} was calculated to be 4 mg/g at 1.2 V with a charge efficiency of 37.3% (Fig. S8a ‡). This value is comparable to lots of carbon based electrode for CDI application.[18] More importantly, the pure CNT used in our experiment just achieve 0.6 mg/g electrosorptive capacity at 1.2 V

(Fig.S8b ‡). This signal implies that 1S-H_xMoO_{3-y} nanobelts possess exciting ions electrosorption ability. The regeneration behavior was depicted in the Fig. 4d, apparently, the 1S-H_xMoO_{3-y} electrode demonstrated high stability of adsorption capacity during three consecutive cycles.

Conclusion

In summary, the SnO_2 coated H_xMoO_{3-y} nanobelts were successfully fabricated through one simple step by using $SnCl_2$ to reduce the MoO_3 nanobelts in the acid solution under room temperature. This electrode has been demonstrated excellent electrochemical performance in Li^+ and Mg^{2+} aqueous solution. Moreover, this electrode has good performance with sea water as electrolyte, holding highest volumetric capacitance over 210 F/cm^3 and good cycling stability with capacitance retention of 93.3% after 4000 cycles at the current density of 1 A/g. The symmetric device based on this electrode could deliver highest energy density of 1.1 mWh/cm^3 with a power density of 6.8 W/cm^3. Moreover, this hybrid composite also have exciting electrosorptive capacity around 4 mg/g in the NaCl solution. All the benefits couple with low-cost material, green electrolyte and a comparable destination capability lead this hybrid composite own practical potential not only for energy storage but also for efficient water desalination application.

Acknowledgements

This work was financially supported by the National Natural Science Foundation of China (51322210, 61434001), the China Postdoctoral Science Foundation (2014M550390, 2014M552033) and Director Fund of WNLO. The authors thank to the facility support of the Center for Nanoscale Characterization & Devices, WNLO-HUST and the Analysis and Testing Center of Huazhong University of Science and Technology.

References

1 a) P. Simon, Y. Gogotsi, *Nat. Mater*. **2008**, **7**, 845-854; b) Y. Zhu, S. Murali, M. D. Stoller, K. J. Ganesh, W. Cai, P. J. Ferreira, A. Pirkle, R. M. Wallace, K. A. Cychosz, M. Thommes, D. Su, E. A. Stach, R. S. Ruoff, *Science*, 2011, **332** 1537-1541; c) M. F. El-Kady, V. Strong, S. Dubin, R. B. Kaner, *Science*, 2012, **335**, 1326-1330.

2 a) M. B. Sassin, C. N. Chervin, D. R. Rolison, J. W. Long, *Acc. Chem. Res,* 2012, **46**, 1062-1074; b) D. N. Futaba, K. Hata, T. Yamada, T. Hiraoka, Y. Hayamizu, Y. Kakudate, O. Tanaike, H. Hatori, M. Yumura, S. Iijima, *Nat. Mater*, 2006, **5,** 987-994; c) J. Bae, M. K. Song, Y. J. Park, J. M. Kim, M. Liu, Z. L. Wang, *Angew. Chem. Int. Edit*, 2011, **50***,* 1683-1687.

3 a) J. Chmiola, C. Largeot, P.-L. Taberna, P. Simon, Y. Gogotsi, *Science*, 2010, **328**, 480-483; b) J. R. Miller, R. A. Outlaw, B. C. Holloway, Science, 2010, **329**, 1637-1639.

4 a) Z. Yu, L. Tetard, L. Zhai, J. Thomas, *Energy Environ. Sci*, 2014, DOI: 10.1039/C4EE03229B; b) V. Augustyn, P. Simon, B. Dunn, *Energy Environ. Sci*, 2014, **7**, 1597-1614; c) L. Huang, D. C. Chen, Y. Ding, S. Feng, Z. L.Wang, M. L. Liu, *Nano Lett,* 2013, **13**, 3135−3139; d) L. Huang, D. C. Chen, Y. Ding, Z. L. Wang, Z. Z. Zeng, M. L. Liu, *ACS Appl. Mater. Interfaces,* 2013, **5**, 11159-11162.

5 a) N. A. Chernova, M. Roppolo, A. C. Dillon, M. S. Whittingham, *Journal Of Materials Chemistry*, 2009, **19**, 2526-2552; b) L. Zheng, Y. Xu, D. Jin, Y. Xie, *Chem. Mater*, 2009, **21**, 5681-5690; c) S.-H. Lee, Y.-H. Kim, R. Deshpande, P. A. Parilla, E. Whitney, D. T. Gillaspie, K. M. Jones, A. H. Mahan, S. Zhang, A. C. Dillon, *Adv. Mater*, 2008, **20**, 3627-3632.

6 T. Brezesinski, J. Wang, S. H. Tolbert, B. Dunn, *Nat. Mater*, 2010, **9**, 146-151.

7 a) X. Lu, G. Wang, T. Zhai, M. Yu, J. Gan, Y. Tong, Y. Li, *Nano Lett*, 2012, **12**, 1690-1696; b) X. Lu, T. Zhai, X. Zhang, Y. Shen, L. Yuan, B. Hu, L. Gong, J. Chen, Y. Gao, J. Zhou, Y. Tong, Z. L. Wang, *Adv. Mater*, 2012, **24**, 938-944; c) W. Zhou, J. Zhu, C. Cheng, J. Liu, H. Yang, C. Cong, C. Guan, X. Jia, H. J. Fan, Q. Yan, C. M. Li, T. Yu, *Energy Environ. Sci*, 2011, **4**, 4954; d) X. Xiao, Z. Peng,

C. Chen, C. Zhang, M. Beidaghi, Z. Yang, N. Wu, Y. Huang, L. Miao, Y. Gogotsi, J. Zhou, *Nano Energy*, 2014, **9**, 355-363.

8 a) B. Braïda, S. Adams, E. Canadell, *Chemistry of Materials*, 2005, **17**, 5957-5969; b) X. K. Hu, Y. T. Qian, Z. T. Song, J. R. Huang, R. Cao, J. Q. Xiao, *Chem. Mater*, 2008, **20**, 1527-1533.

9 a) G. Yu, X. Xie, L. Pan, Z. Bao, Y. Cui, *Nano Energy*, 2013, **2**, 213-234; b) G. Sun, J. Liu, X. Zhang, X. Wang, H. Li, Y. Yu, W. Huang, H. Zhang, P. Chen, *Angew. Chem. Int. Edit*, 2014, **53**, 12576-12580; c) Y. Zhang, W. Bai, X. Cheng, J. Ren, W. Weng, P. Chen, X. Fang, Z. Zhang, H. Peng, *Angew. Chem. Int. Edit*, 2014, **53**, 14564-14568.

10 a) K. Fic, G. Lota, M. Meller, E. Frackowiak, *Energy Environ. Sci*, 2012, **5**, 5842-5850; b) M. P. Bichat, E. Raymundo-Piñero, F. Béguin, *Carbon,* 2010, **48**, 4351-4361.

11 M. H. Sharqawya, J. H. Lienhard Va, S. M. Zubair, *Desalin. Water Treat*, 2010, **10**, 354-380.

12 M. Pasta, C. D. Wessells, Y. Cui, F. La Mantia, *Nano Lett*, 2012, **12**, 839-843

13 a) Z. Wang, D. Luan, F. Y. Boey, X. W. Lou, *J. Am. Chem. Soc*, 2011, **133**, 4738-4741; b) X.-Y. Xue, Z.-H. Chen, L.-L. Xing, S. Yuan, Y.-J. Chen, *Chem. Commun*, 2011, **47**, 5205-5207.

14 a) X. Yang, C. Cheng, Y. Wang, L. Qiu, D. Li, *Science*, 2013, **341**, 534-537; b) M. Heon, S. Lofland, J. Applegate, R. Nolte, E. Cortes, J. D. Hettinger, P.-L. Taberna, P. Simon, P. Huang, M. Brunet, Y. Gogotsi, *Energy Environ. Sci*, 2011, **4**, 135-138.

15 V. Augustyn, J. Come, M. A. Lowe, J. W. Kim, P.-L. Taberna, S. H. Tolbert, H. D. Abruña, P. Simon, B. Dunn, *Nat. Mater*, 2013, **12**, 518-522.

16 a) A. C. Sun, W. Kosar, Y. Zhang, X. Feng, *J. Membrane. Sci,* 2014, **455**, 131-142; b) V. V. Nikonenko, A. V. Kovalenko, M. K. Urtenov, N. D. Pismenskaya, J. Han, P. Sistat, G. Pourcelly, *Desalination,* 2014, **342**, 85-106; c) A. Drak, M. Adato, *Desalination*, 2014, **339**, 34-39.

17 S. Porada, R. Zhao, A. van der Wal, V. Presser, P. M. Biesheuvel, *Prog. Mater. Sci*, 2013, **58**, 1388-1442.

18 a) K. Dai, L. Shi, J. Fang, D. Zhang, B. Yu, *Mater. Lett*, 2005, **59**, 1989-1992; b) H. Li, L. Pan, C. Nie, Y. Liu, Z. Sun, *J. Mater. Chem*, 2012, **22**, 15556-15561; c) X. Z. Wang, M. G. Li, Y. W. Chen, R. M. Cheng, S. M. Huang, L. K. Pan, Z. Sun, Electrochem. *Solid-State Lett*, 2006, **9**, E23-E26.

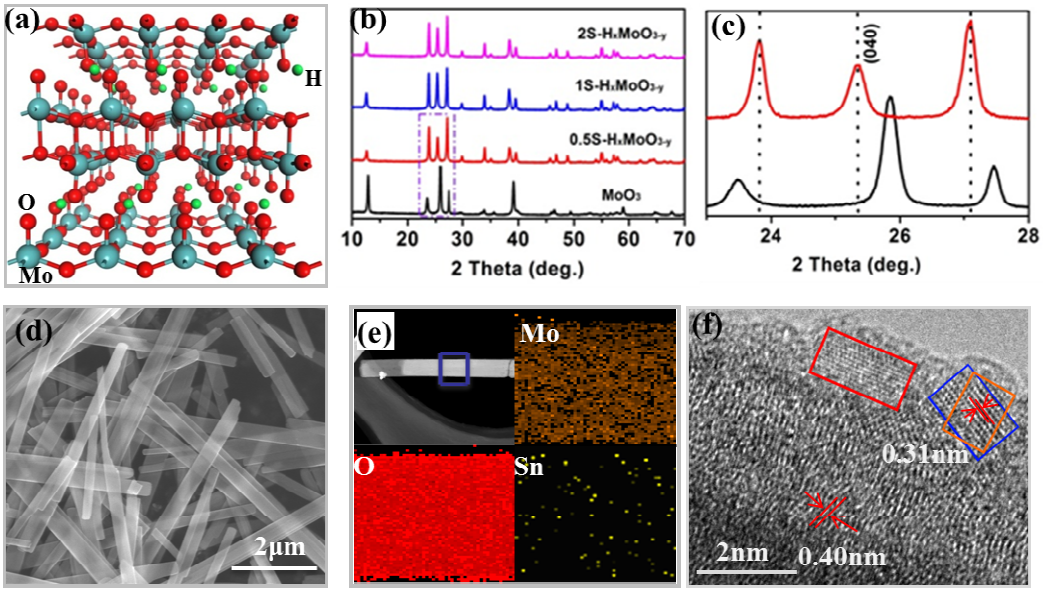

Fig. 1 (a) Crytstalline structure of H_xMoO_{3-y}; (b) (c) XRD of H_xMoO_{3-y} with different reduction time (d) SEM and (e) element mapping of 1S-H_xMoO_{3-y}; (f) HRTEM images of 1S-H_xMoO_{3-y}.

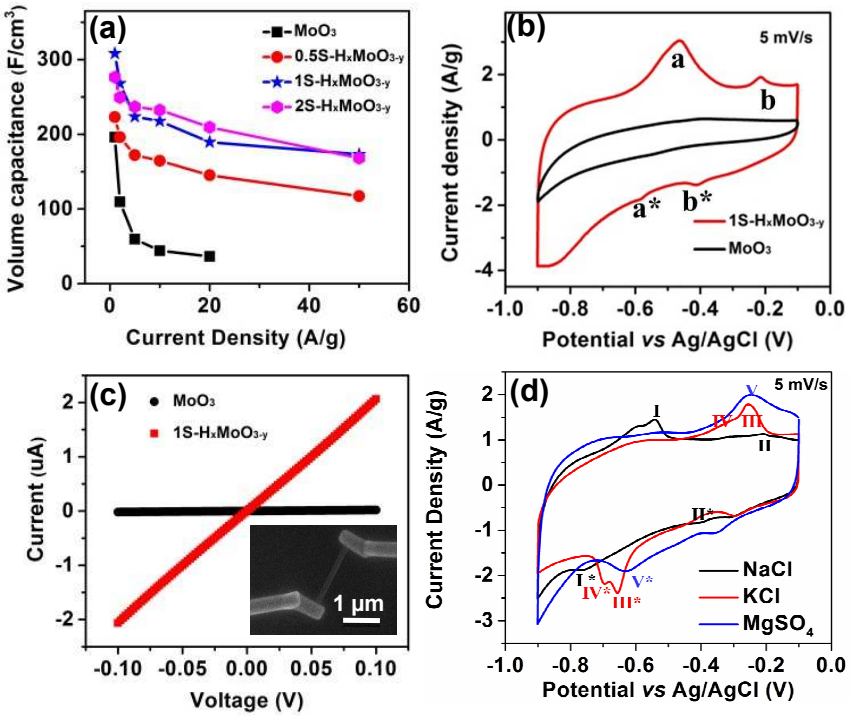

Fig. 2 (a) Volumetric capacitance of MoO_3, 0.5S-H_xMoO_{3-y}, 1S-H_xMoO_{3-y} and 2S-H_xMoO_{3-y}; (b) CV curves of 1S-H_xMoO_{3-y} and pristine MoO_3 at seep rate of 5mV/s in the 5 M LiCl solution; (c) I-V curves of MoO_3 and 1 S-H_xMoO_{3-y}; (d) CV curves of 1S-H_xMoO_{3-y} at sweep rate of 5 mV/s by using NaCl, KCl and $MgSO_4$ as electrolyte.

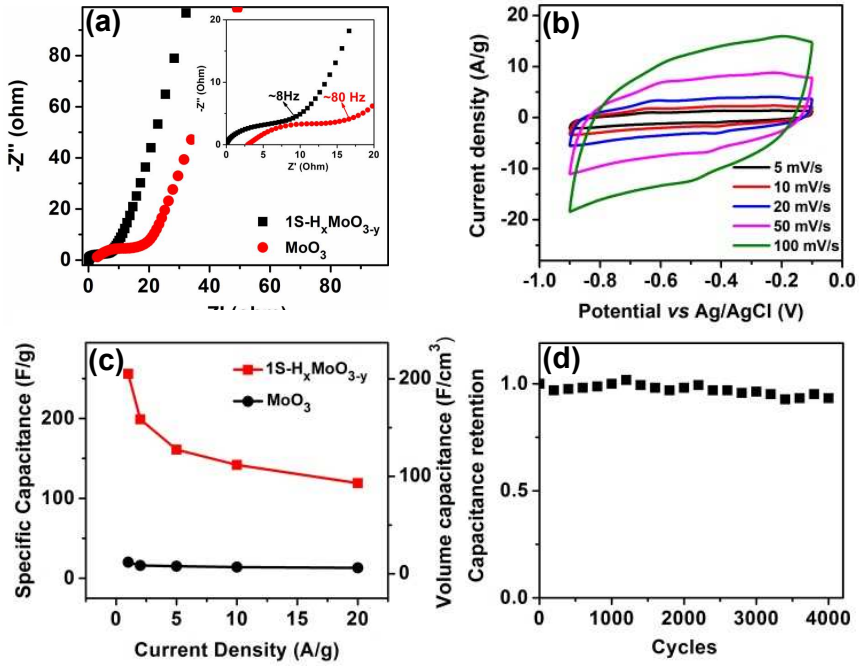

Fig. 3 (a) ESI data of 1S-H_xMoO_{3-y} and MoO_3; (b) CV curves of 1S-H_xMoO_{3-y} by using sea water as electrolyte under various sweep rate; (c)specific capacitance of 1S-H_xMoO_{3-y} and MoO_3 in the sea water; (d) cycling stability of 1S-H_xMoO_{3-y} at 1 A/g.

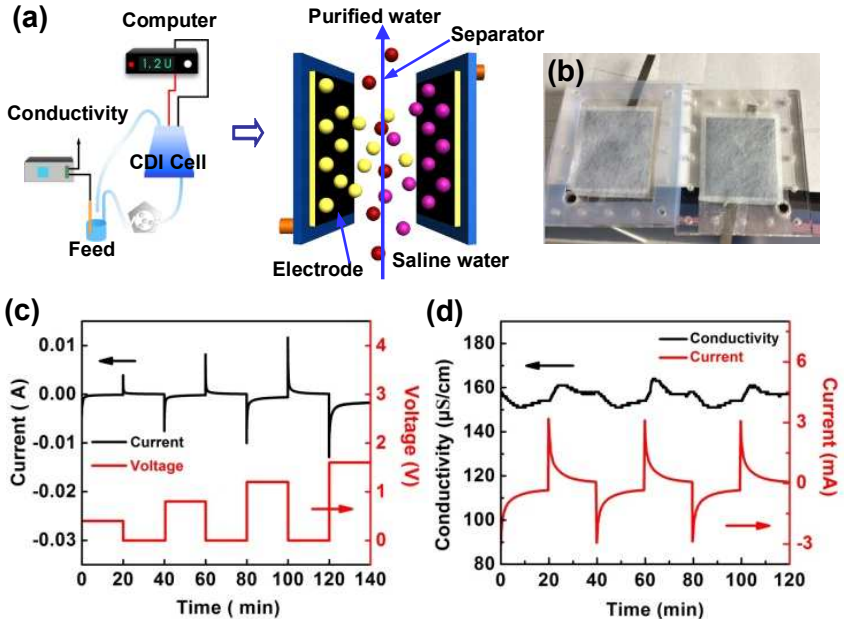

Fig. 4 (a) The schematic of CDI process; (b) specific electrode membrane used in our experiment; (c) The current response of the 1S-H_xMoO_{3-y} and CNT hybrid electrode in NaCl solution by varying the cell voltage from 0.4 to 1.6 V; (d) Desalination performance and regeneration plot for the 1S-H_xMoO_{3-y} and CNT hybrid electrode under cell potential of 1.2 V in NaCl solution with flow rate of 20 mL/min.